A weighted essentially non-oscillatory numerical scheme for a multi-class traffic flow model on an inhomogeneous highway *

Peng Zhang[1,2] S.C. Wong[1†] and Chi-Wang Shu[3]

1. Department of Civil Engineering, The University of Hong Kong, Hong Kong SAR, P.R. China

2. Shanghai Institute of Applied Mathematics and Mechanics, Shanghai, P.R.China

3. Division of Applied Mathematics, Brown University, Providence, RI 02912, USA

Abstract: As a new attempt to solve hyperbolic conservation laws with spatially varying fluxes, the weighted essentially non-oscillatory (WENO) method is applied to solve a multi-class traffic flow model for an inhomogeneous highway. The numerical scheme is based upon a modified equivalent system that is written in a "standard" hyperbolic conservation form. Numerical examples, which include the difficult traffic signal control problem, are used to demonstrate the effectiveness of the WENO scheme.

Keywords: non-strictly hyperbolic conservation laws; spatially varying fluxes; WENO reconstruction

1 Introduction

In this paper, we extend a multi-class Lighthill-Whitham-Richards traffic flow model [21,23,28] to deal with inhomogeneous road conditions. The variable road conditions are the number of lanes $a(x)$ and the free flow (maximum) velocities $\{v_{l,f}(x)\}_{l=1}^m$ of m types of vehicles. Let $\rho_l(x,t)$ be the density per lane of the lth type, and let

$$\rho(x,t) = \sum_{l=1}^{m} \rho_l(x,t)$$

be the total density per lane. The velocity of the lth type of vehicles is a function of ρ, which is denoted by $v_l(\rho)$. Furthermore we assume that $\{v_l\}_{l=1}^m$ are related by

$$v_l = b_l(x)v(\rho),\ v'(\rho) < 0,\ b_l(x) = v_{l,f}(x)/v_f,\ v_f = \max_x \max_{1\le l\le m}(v_{l,f}(x)). \tag{1.1}$$

*The work described in this paper was jointly supported by grants from the Hong Kong Research Grants Council of the Hong Kong Special Administrative Region, China (Project No. HKU 7031/02E) and the National Natural Science Foundation of China (Project No. 10472064). The research of the third author was supported by NSF grant DMS-0207451 and ARO grant W911NF-04-1-0291.

†Corresponding author. E-mail: hhecwsc@hkucc.hku.hk.

Accordingly, the velocity differences between m vehicle types are reflected by the functions $\{b_l(x)\}_{l=1}^m$ and $0 \le b_l(x) \le 1$.

The model equations are acquired from the mass conservation of m types of vehicles, which read

$$(a(x)\rho_l)_t + (a(x)\rho_l b_l(x)v(\rho))_x = 0, \quad 1 \le l \le m. \tag{1.2}$$

We introduce the conservative solution variables $u_l = a(x)\rho_l$, the vector $u = (u_1, \ldots, u_m)^T$, and the flux vector $f = (f_1, \ldots, f_m)^T$ with $f_l = b_l u_l v(\Sigma u_l/a)$. Accordingly, the model equations can be written as

$$u_t + f(u, \theta(x))_x = 0, \tag{1.3}$$

where the vector function $\theta(x)$ represents all inhomogeneous factors on the road, namely,

$$\theta(x) = (a(x), b_1(x), \ldots, b_m(x)).$$

In this traffic flow problem, each density ρ_l and the total density ρ are bounded by a jam density ρ_{jam}, and thus

$$u/a \in \bar{D}, \quad \bar{D} = \{u/a|\ \rho_l \ge 0,\ l = 1, \ldots, m; \Sigma_{l=1}^m \rho_l \le \rho_{jam}\}. \tag{1.4}$$

Moreover, the function $v(\rho)$ of (1.1) satisfies

$$v(0) = v_f, \quad v(\rho_{jam}) = 0.$$

The study of this extended traffic flow system is significant both for practical application and theoretical interest. In real traffic, the drop or increase in traffic capacity that is reflected by $\theta(x)$ is frequent in many locations, such as on curves and slopes and near ramps and traffic accidents. In particular, by extension $b_l = b_l(x,t)$ can serve as a switch function in signal traffic or the like. However, it is very difficult to solve the eigen-polynomial of system (1.3) explicitly. Moreover, the existence of spatially varying fluxes poses significant difficulties for both analytical and numerical studies (see [1-2], [10], [14-15], and [24-27] for relevant discussions).

In this paper, some important features of the model are discussed under a modified equivalent system of (1.3), in which all of the components of θ are solution variables. Analytically, the hyperbolicity of the system is proven, and the wave-breaking patterns of the Riemann problem are predicted. We note that these descriptions are mostly based on the relevant studies in [24] and [28]. The maximum absolute value of all of the eigenvalues is estimated, which is an essential parameter in the proposed numerical schemes. We note that these eigenvalues cannot be explicitly solved (see Section 2 for this discussion).

In developing the numerical schemes, it may not be efficient to apply the standard methods (e.g., TVD, RKDG, and WENO schemes) to system (1.3) directly due to its spatially varying fluxes. It

should be mentioned that a wave propagation method was recently developed that generated good numerical results in solving elastic waves in heterogeneous media, which constitute a 2×2 system with spatially varying fluxes [2]. Nevertheless, this method is limited to problems in which an eigenvalue has a fixed sign for all involved u and $\theta(x)$, and requires that the eigenvalues can be solved explicitly. Therefore, this method is not suitable for our problem, in which one of the eigenvalues changes sign, and all are implicit. In [24-27], Zhang et al. developed a numerical scheme to deal with spatially varying fluxes for the scalar case, which can also be extended to the vector case.

With a modified equivalent system of (1.3), a component-wise WENO scheme that applies the Lax-Friedrichs numerical flux in the finite volume method and the flux splitting in the finite difference method are discussed in Section 3. As the modification gives rise to a standard hyperbolic conservation form, the scheme is theoretically sound, and thus gives good results. Although the Riemann problem of the system generates very complicated wave structures, the numerical results are in good agreement with the claimed wave patterns (Section 4.1). For sharp changes of b_l from their maxima to minima, which describes the sharp braking of vehicles, the resultant strong discontinuity at the interface is well captured (Section 4.2). We note that this is the first time that the WENO scheme has been applied to hyperbolic conservation laws with spatially varying fluxes. Similar applications to other problems may be possible, which is addressed in Section 5 with several concluding remarks.

2 Hyperbolicity and wave structure of the model equations

To study the hyperbolicity and solution structure of the system, we rewrite (1.3) in the "standard" conservation form, which means that we add the identity $\theta_t = 0$ to (1.3). For convenience, we treat θ as a scalar in the following discussions, but the results are equally applicable to the vector case. Accordingly, (1.3) and the added identity can be viewed as the following equivalent $(m+1)\times(m+1)$ system:

$$U_t + F_x = 0, \tag{2.1}$$

where $U = (u, \theta)^T$ and $F = (f(u, \theta), 0)^T$. We note that the construction of equivalent forms of the conservation laws with spatially varying fluxes is widely applied, for example in [1,10,15,25]. According to this standard conservation form, we study the hyperbolicity of the system. We write the Jacobian F_U and the matrix for solving the eigen-pairs as follows:

$$F_U = \begin{pmatrix} f_u & f_\theta \\ \mathbf{0} & 0 \end{pmatrix}, \quad F_U - \lambda I_{m+1} = \begin{pmatrix} f_u - \lambda I_m & f_\theta \\ \mathbf{0} & -\lambda \end{pmatrix}, \tag{2.2}$$

where $\mathbf{0} = (0, \ldots, 0)$ has m components, $f_\theta = (f_{1\theta}, \ldots, f_{m\theta})^T$ and I_m is the unit matrix. Let

$$|f_u - \lambda I_m| = P_m(\lambda),$$

and then the eigen-polynomial of F_U is

$$|F_U - \lambda I_{m+1}| = -\lambda P_m(\lambda). \tag{2.3}$$

2.1 Hyperbolicity of the model equations

For the discussed system, it is not difficult to obtain [28]

$$P_m(\lambda) = Q(\lambda)\prod_{l=1}^{m}(v_l - \lambda), \quad Q(\lambda) = 1 + \sum_{l=1}^{m}\frac{\rho_l}{v_l - \lambda}\frac{\partial v_l}{\partial \rho}. \tag{2.4}$$

For $u/a \in D$, where D is the open domain that corresponds to $\bar{D}$ of (1.4), we suppose that $\{v_l\}_{l=1}^m$ are distinct, namely,

$$v_1 < \ldots < v_m, \tag{2.5}$$

then it is easy to verify that, by (2.4),

$$sgn(P_m(v_l)) = (-1)^l, \quad sgn(P_m(v_1 + \sum_{l=1}^{m}\rho_l\frac{\partial v_l}{\partial \rho})) = 1. \tag{2.6}$$

By the intermediate value theorem, (2.6) suggests m distinct real eigenvalues $\{\lambda\}_{l=1}^m$ of the Jacobian f_u, which are separated by m velocities as follows:

$$v_1 + \sum_{l=1}^{m}\rho_l\frac{\partial v_l}{\partial \rho} < \lambda_1 < v_1 < \lambda_2 < \ldots < v_{l-1} < \lambda_l < v_l < \ldots < v_{m-1} < \lambda_m < v_m. \tag{2.7}$$

For $u/a \in \partial D$, m real eigenvalues of f_u are also ensured, and some inequalities of (2.7) change to equalities. The hyperbolicity of this latter case is rather complicated, but to a degree can be viewed as the limiting case of the former (see [28] for more details). For simplicity, this case is excluded from this section and from Section 2.2.

By (2.3), therefore, we conclude that the Jacobian F_u has $m+1$ real eigenvalues $\{\lambda_l\}_{l=1}^m$ and that $\tilde{\lambda} = 0$, and thus that (2.1) is a hyperbolic system. Furthermore, by (2.7) it is obvious that these $m+1$ eigenvalues are distinct if and only if $\lambda_1 \neq \tilde{\lambda} = 0$, in which case (2.1) is strictly hyperbolic. As is shown in the following, it is possible to have $\lambda_1 = \tilde{\lambda} = 0$, in which case system (2.1) is generally non-strictly hyperbolic.

Substituting λ with $\lambda_1 = 0$ in (2.4) and with all v_l being given by (1.1), we have

$$Q(0) = \frac{q'(\rho)}{v(\rho)}, \quad sgn(P_m(0)) = sgn(q'(\rho)), \tag{2.8}$$

where $q(\rho) = \rho v(\rho)$. Usually, $q(\rho)$ is supposed to be strictly concave [21,23,28], $q''(\rho) < 0$. Assume that $q(\rho^*)$ is the maximum of $q(\rho)$, such that

$$q'(\rho^*) = 0,\ q'(\rho) > 0\ for\ \rho < \rho^*,\ q'(\rho) < 0\ for\ \rho > \rho^*,$$

where ρ^* is the critical density, as it is called in many traffic flow models. Accordingly, (2.8) and (2.6) give the following conclusion:

$$\lambda_1 \begin{cases} > 0, & if \quad \rho < \rho^*, \\ = 0, & if \quad \rho = \rho^*, \\ < 0, & if \quad \rho > \rho^*. \end{cases} \tag{2.9}$$

This is again derived by the intermediate value theorem.

Suppose that $(r_l^T, z_l)^T$ is an eigenvector that corresponds to λ_l, where r_l is a $m \times 1$ vector and z_l is a scalar, then we have

$$\lambda = \lambda_l : \ (F_U - \lambda_l I_{m+1}) \begin{pmatrix} r_l \\ z_l \end{pmatrix} = \begin{pmatrix} f_u - \lambda_l I_m & f_\theta \\ \mathbf{0} & -\lambda_l \end{pmatrix} \begin{pmatrix} r_l \\ z_l \end{pmatrix} = \begin{pmatrix} (f_u - \lambda_l I_m) r_l + z_l f_\theta \\ -\lambda_l z_l \end{pmatrix} = 0.$$

This indicates that we can take z_l to be zero and r_l to be the eigenvector of f_u that corresponds to λ_l.

Suppose that $(\tilde{r}^T, \tilde{z})^T$ is an eigenvector that corresponds to $\tilde{\lambda} = 0$. Similarly, we have

$$\tilde{\lambda} = 0 : \quad (F_U - \tilde{\lambda} I_{m+1}) \begin{pmatrix} \tilde{r} \\ \tilde{z} \end{pmatrix} = \begin{pmatrix} f_u & f_\theta \\ \mathbf{0} & 0 \end{pmatrix} \begin{pmatrix} \tilde{r} \\ \tilde{z} \end{pmatrix} = \begin{pmatrix} f_u \tilde{r} + \tilde{z} f_\theta \\ 0 \end{pmatrix} = 0,$$

which implies that $\tilde{r}$ is the solution of the algebraic equations

$$f_u \tilde{r} = -\tilde{z} f_\theta. \tag{2.10}$$

Denote by $r = (r_1, \ldots, r_m)$ a non-singular matrix of right-eigenvectors of f_u. The matrix of the right-eigenvectors of F_U then reads

$$R \equiv \begin{pmatrix} r & \tilde{r} \\ \mathbf{0} & \tilde{z} \end{pmatrix}.$$

If $\lambda_1 \neq 0$, then f_u is non-singular. We choose $\tilde{z} \neq 0$ in (2.10), and thus $\tilde{r}$ is uniquely determined as $\tilde{r} = -\tilde{z} f_u^{-1} f_\theta$. In this case R is non-singular and

$$R = \begin{pmatrix} r & -\tilde{z} f_u^{-1} f_\theta \\ \mathbf{0} & \tilde{z} \end{pmatrix}, \quad R^{-1} = \begin{pmatrix} r^{-1} & r^{-1} f_u^{-1} f_\theta \\ \mathbf{0} & 1/\tilde{z} \end{pmatrix}.$$

If $\lambda_1 = 0$, then f_u is singular. Consequently, R must be singular. This is obvious for $\tilde{z} = 0$. For $\tilde{z} \neq 0$, if Eq.(2.10) has a solution to $\tilde{r}$, then we would read $rank(f_u, -\tilde{z} f_\theta) = rank(f_u) = rank(f_u - \lambda_1 I_m) = m - 1$, for which an identity is required. This is generally unlikely under the assumption that $f_\theta \neq 0$. For the discussed traffic flow problem, the required identity can be arranged as

$$\sum_{l=1}^{m} \frac{\partial f_l}{\partial x} \frac{1}{v_l} \equiv 0, \quad or \quad a \sum_{l=1}^{m} \frac{b_l'}{b_l} \rho_l - \frac{v'}{v} \rho^2 a' \equiv 0, \ for \ \lambda_1 = 0, \ or \ \rho = \rho^*.$$

However, it is obvious that this condition does not hold for the traffic flow model.

In summary, system (2.1) is strictly hyperbolic for $\lambda_1 \neq 0$, but non-strictly hyperbolic for $\lambda_1 = 0$.

2.2 Wave structure of the model equations

We consider the Riemann problem

$$u = \begin{cases} u^1, & if \quad x < 0, \\ u^{m+1}, & if \quad x > 0, \end{cases} \qquad \theta = \begin{cases} \theta^L, & if \quad x < 0, \\ \theta^R, & if \quad x > 0, \end{cases} \tag{2.11}$$

where the expression for θ means that $a(x)$ and $b_l(x)$ are discontinuous of x at the interface, with $\theta^L = (a^L, b_1^L, \ldots, b_m^L)$, and $\theta^R = (a^R, b_1^R, \ldots, b_m^R)$.

The Riemann problem was solved exactly for a general scalar form of (1.3) ($m = 1$) in [24]. For the case $m = 2$, λ_1 and λ_2 are explicit, but the solution is very complicated. For $m > 2$, no λ_l can be solved explicitly in the discussed traffic flow problem, and thus it is very difficult to derive the analytical results [28]. However, some predictions of the wave structure are possible, because the wave breaking near the interface would be similar to that for the scalar case that is discussed in [24]. Moreover, the monotone changes across or within the waves other than the interface are well understood for the system in which $\theta(x)$ is constant [28], and these conclusions are still applicable in each of the regions $D^+ = \{(x,t)|x > 0,\ t > 0\}$ and $D^- = \{(x,t)|x < 0,\ t > 0\}$. The claimed wave structure in this section serves as a comparison for the numerical results in Section 3.

We call a wave that corresponds to the λ_l- (or $\tilde{\lambda}$-) characteristic field the λ_l- (or $\tilde{\lambda}$-) wave. In accordance with (2.7), these $\{\lambda_l\}_{l=2}^m$-waves must be in the region $D^+ = \{(x,t)|x > 0,\ t > 0\}$, and the $\tilde{\lambda}$-wave can be easily verified as a contact at the interface $x = 0$. See [11-13,18-20] for detailed accounts of the basic properties of hyperbolic waves. Let $u^L = u(0, t^-)$ and $u^R = u(0, t^+)$, which are, respectively, the left and right solution states that are adjacent to the interface, and we then have, by the *Rankine-Hugoniot* jump condition,

$$f(u^L, \theta^L) = f(u^R, \theta^R). \tag{2.12}$$

As indicated in [24], the two states u^L and u^R should be also "connected" by the λ_l characteristics. This argument implies that the propagation of the λ_1-characteristics may change the angle across the interface, and should satisfy

$$\lambda_1(u^L, \theta^L)\lambda_1(u^R, \theta^R) \geq 0. \tag{2.13}$$

Here, the equality means that $\lambda_1(u^L, \theta^L)$ or $\lambda_1(u^R, \theta^R)$ coincides with the contact $\tilde{\lambda} = 0$, in which case system (2.1) must be non-strictly hyperbolic. We have, by (2.12),

$$a^L b_l^L \rho_l^L v(\rho^L) = a^R b_l^R \rho_l^R v(\rho^R), \quad l = 1, \ldots, m.$$

Let $\alpha_{1l} = a^L b_l^L/(a^R b_l^R)$ and $\alpha_{2l} = 1/\alpha_{1l}$, and the aforementioned equation is then equivalent to

$$\rho_l^R v(\rho^R) = \alpha_{1l}\rho_l^L v(\rho^L), \quad \forall l; \quad \rho^R v(\rho^R) = v(\rho^L)\sum_{l=1}^m \alpha_{1l}\rho_l^L, \tag{2.14}$$

where the second equation is obtained by the summation of the first over l. Similarly, we obtain

$$\rho_l^L v(\rho^L) = \alpha_{2l}\rho_l^R v(\rho^R), \quad \forall l; \quad \rho^L v(\rho^L) = v(\rho^R)\sum_{l=1}^{m}\alpha_{2l}\rho_l^R. \tag{2.15}$$

In the discussed traffic flow problem, it is reasonable to assume that

$$if\ \alpha_{1k} > 1\ for\ some\ k, \quad then\ \alpha_{1l} \geq 1 \ \ \forall\ l, \tag{2.16}$$

which indicates a non-increase or non-decrease ($\alpha_{1l} \geq 1$ or $\alpha_{1l} \leq 1$) in traffic capacity for all types of vehicles. Otherwise, the problem would be unrealistic, because the capacity drops for some vehicle types but increases for others in the same location.

Whether system (2.1) is strictly hyperbolic will be subject to (2.13), because $\theta(x)$ is only changeable across the interface. Let u^2 be the left solution state of the λ_2-wave (Figs.1 and 2), and we then have the following description.

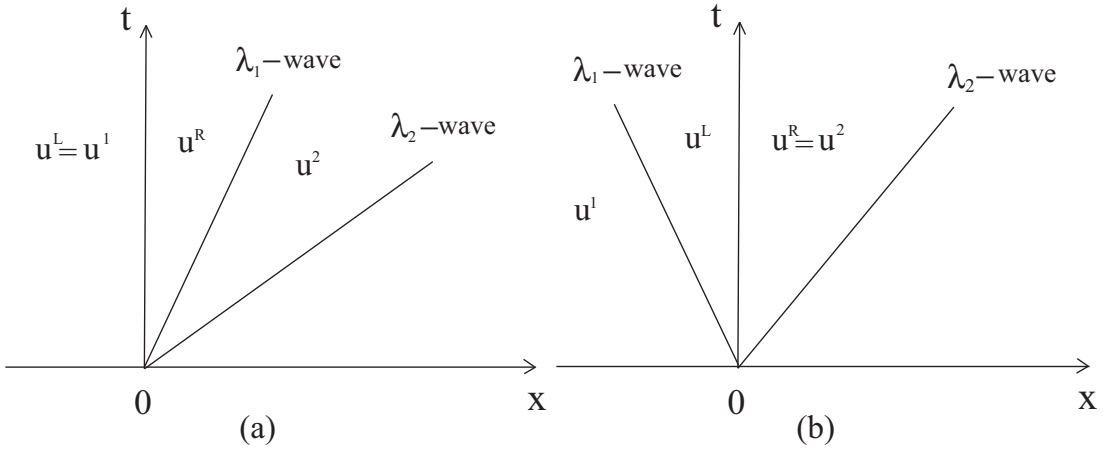

Fig.1 Wave patterns that correspond to a strictly hyperbolic system (2.1): (a) the λ_1-characteristics pass through the interface from left to right; (b) the λ_1-characteristics pass through the interface from right to left.

(1) Suppose that $\lambda_1(u^L, \theta^L)\lambda_1(u^R, \theta^R) > 0$, then system (2.1) is strictly hyperbolic and we would expect $m+1$ waves. In addition to the $\tilde{\lambda}$-contact at the interface, only one λ_1-wave is needed before the λ_2-wave. This λ_1-wave is either in D^+ or D^- for the consideration of the following three cases.

(a) If $\lambda_1(u^1, \theta^L) > 0$ and $\lambda_1(u^2, \theta^R) \geq 0$, then it is natural to have $u^L = u^1$ and $\lambda_1(u^L, \theta^L) > 0$. As $\lambda_1(u^R, \theta^R) > 0$, it is inferred by (2.9) that $\rho^R < \rho^*$. Such a unique ρ^R and the components of u^R are solvable by (2.14) if and only if

$$v(\rho^L)\sum_{l=1}^{m}\alpha_{1l}\rho_l^L < \rho^* v(\rho^*) = q(\rho^*). \tag{2.17}$$

In this case we can say that the propagation of $\lambda_1(u^1, \theta^L)$ is able to pass through the interface and then change to $\lambda_1(u^R, \theta^R)$, in which state u^R forms the λ_1-wave with u^2 in D^+. Fig.1(a) shows this wave pattern, where a wave is represented simply by a radial.

(b) If $\lambda_1(u^1, \theta^L) \le 0$ and $\lambda_1(u^2, \theta^R) < 0$, then similarly we have $u^R = u^2$ and $\lambda_1(u^R, \theta^R) < 0$, and thus $\lambda_1(u^L, \theta^L) < 0$ and $\rho^L > \rho^*$. By (2.15), ρ^L and $\{\rho_l^L\}_{l=1}^m$ are uniquely solvable if and only if

$$v(\rho^R) \sum_{l=1}^{m} \alpha_{2l} \rho_l^R < \rho^* v(\rho^*) = q(\rho^*). \tag{2.18}$$

In this case, we can say that the propagation of $\lambda_1(u^2, \theta^R)$ is able to pass through the interface and then change to $\lambda_1(u^L, \theta^L)$, in which state u^L forms the λ_1-wave with u^1 in D^-. This wave pattern is shown in Fig.1(b).

(c) If $\lambda_1(u^1, \theta^L) > 0$ and $\lambda_1(u^2, \theta^R) < 0$, then we have either $u^L = u^1$ or $u^R = u^2$. Accordingly, the wave pattern is similar to that of (1)(a) or (b), as is shown in Figs.1(a) and (b). We note that at least one of Eqs. (2.14) (with $u^L = u^1$) and (2.15) (with $u^R = u^2$) is solvable, because at least one of conditions (2.17) (with $u^L = u^1$) and (2.18) (with $u^R = u^2$) must hold under assumption (2.16).

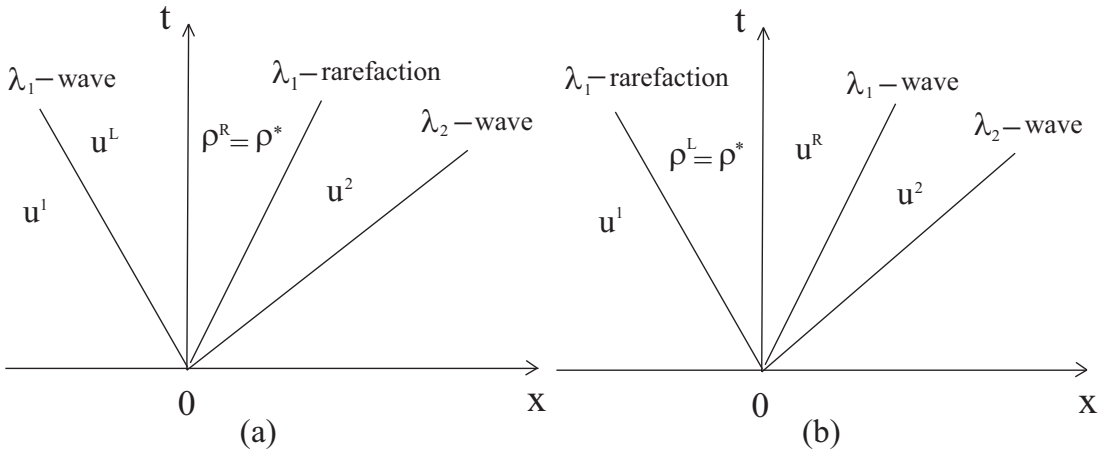

Fig.2 Wave patterns that correspond to a non-strictly hyperbolic system (2.1): (a) the λ_1-characteristics of $u = u^1$ are reflected from the interface, forming an extra λ_1-wave in D^-; (b) the λ_1-characteristics of $u = u^2$ are reflected from the interface, forming an extra λ_1-wave in D^+.

(2) Suppose that $\lambda(u^L, \theta^L)\lambda(u^R, \theta^R) = 0$, then system (2.1) is non-strictly hyperbolic and we predict a total of $m+2$ waves in the following. For all of the cases under consideration, we need two λ_1-waves that are separated by the interface. This wave structure is also characterized by a λ_1-rarefaction, which is either in D^- or in D^+, and is distinguished by two wave patterns that are shown in Figs.2(a) and (b), respectively.

(a) If $\lambda_1(u^1,\theta^L) > 0$, $\lambda_1(u^2,\theta^R) \geq 0$, and (2.17) is not satisfied for $u^L = u^1$ so that (2.14) is unsolvable (except possibly for $\rho^R = \rho^*$), then by the assumption we can only choose $\lambda_1(u^R,\theta^R) = 0$, namely $\rho^R = \rho^*$. Moreover, by (2.14) and (2.15), we have

$$v(\rho^L)\sum_{l=1}^{m}\alpha_{1l}\rho_l^L = \rho^* v(\rho^*) = q(\rho^*), \quad \rho^L v(\rho^L) = v(\rho^*)\sum_{l=1}^{m}\alpha_{2l}\rho_l^R. \tag{2.19}$$

Comparing the first equation of (2.19) with (2.17), we can see that a maximal principle is applied. The second equation of (2.19) is solvable, because it is implied that $\alpha_{2l} \leq 1$ ($\alpha_{1l} \geq 1$) for all l, and thus $v(\rho^*)\Sigma_{l=1}^m\alpha_{2l}\rho_l^R \leq v(\rho^*)\rho^* = q(\rho^*)$. Otherwise, by (2.16), we have $\alpha_{1l} \leq 1$ for all l, and (2.17) will be satisfied by $u^L = u^1$. However, this contradicts our assumption.

In this case, ρ^L is chosen such that $\lambda(u^L,\theta^L) \leq 0$, namely $\rho^L \geq \rho^*$. Therefore, the propagation of $\lambda_1(u^1,\theta^L)$ is unable to pass through the interface, and reflects backward so that u^1 and u^L form a λ_1-wave in D^-. Meanwhile, u^R and u^2 form another λ_1-wave that can be identified as a rarefaction (see Proposition 2.2), because $\rho^R = \rho^* > \rho^2$. This wave pattern is shown in Fig.2(a).

(b) If $\lambda_1(u^1,\theta^L) \leq 0$, $\lambda_1(u^2,\theta^R) < 0$, and (2.18) is not satisfied for $u^R = u^2$ so that (2.15) is unsolvable (except possibly for $\rho^L = \rho^*$), then we have $\lambda(u^L,\theta^L) = 0$ or $\rho^L = \rho^*$. This case is parallel to (1)(a), and the wave structure is shown in Fig.2(b), where two predicted λ_1-waves are also separated by the interface. In contrast to 2(a), here it is the λ_1-wave in D^- that is identified as a rarefaction (also see Proposition 2.2), because $\rho^1 > \rho^L = \rho^*$.

(c) If $\lambda_1(u^1,\theta^L) < 0$ and $\lambda_1(u^2,\theta^R) > 0$, which suggests that $\lambda_1(u,\theta)$ changes sign across the interface, then we have $\lambda_1(u^R,\theta^R) = 0$ for $\alpha_{1l} \geq 1$. In this case, the wave structure is similar to that of (2)(a), and is also shown in Fig.2(a). For $\alpha_{2l} \geq 1$, we have $\lambda_1(u^L,\theta^L) = 0$, and the wave pattern is similar to that of (2)(b), as shown in Fig.2(b). We have the trivial case of this for $\lambda_1(u^1,\theta^L) = 0$ or $\lambda_1(u^2,\theta^R) = 0$.

For the scalar case $m = 1$, in which the λ_l-waves disappear for $l > 1$ and $u^2 = u^{m+1}$ becomes known initially, the wave patterns as shown in Figs.1 and 2 are identical to those that were solved exactly and proved to be unique in [24]. Furthermore, the conclusions for all of the λ_l-waves in [28] can be directly applied in this Riemann problem, because each of the waves is either in D^- or in D^+, where $\theta(x)$ is constant. In general, all of these λ_l-characteristic fields are genuinely nonlinear, and thus they correspond to either shocks or rarefactions. Let u^- and u^+ be the left and right states of a certain λ_l-wave, respectively, and, supposing that the function $v(\rho)$ is concave, namely, $v''(\rho) \leq 0$, then the following two propositions in [28] may be cited.

Proposition 2.1 *A λ_l-shock is characterized by the following: $\rho^- < \rho^+$, $\rho_k^- < \rho_k^+$ for $k \geq l$ and $\rho_k^- > \rho_k^+$ for $k < l$.*

Proposition 2.2 *A λ_l-rarefaction is characterized by the following: $\rho^- > \rho^+$, $\rho_k^- > \rho_k^+$ for $k \geq l$ and $\rho_k^- < \rho_k^+$ for $k < l$. Moreover, all of the functions $\rho(\theta)$ and $\rho_k(\theta)$ are monotone in the rarefaction fan, where $\theta = x/t$.*

It was also indicated in [28] that the two propositions should be applicable to a generally given function $v(\rho)$.

3 Numerical schemes

For the numerical approximation of the model equations, we follow the basic ideas that are stated in Section 1. We first apply the modified equivalent system (2.1), which is written in two parts as follows:

$$\begin{aligned} u_t + f(u,\theta)_x &= 0, \\ \theta_t + o_x &= 0, \end{aligned} \tag{3.1}$$

where the flux $o = 0$. We note that θ is a solution vector for temporal evolution in the computation. Let $\hat{f}$ and $\hat{o}$ be the two numerical flux functions that correspond to the fluxes f and o, respectively, of (3.1). Then, a standard conservative scheme of (3.1) reads:

$$\begin{aligned} \frac{du_i}{dt} + \frac{1}{\Delta x}(\hat{f}_{i+1/2} - \hat{f}_{i-1/2}) &= 0, \\ \frac{d\theta_i}{dt} + \frac{1}{\Delta x}(\hat{o}_{i+1/2} - \hat{o}_{i-1/2}) &= 0. \end{aligned} \tag{3.2}$$

In the following, the numerical fluxes $\hat{f}_{i+1/2}$ and $\hat{o}_{i+1/2}$ are reconstructed by the WENO method through the Lax-Friedrichs flux splitting method. As the characteristic decomposition of the system is impossible due to the implicitness of all of the λ_l, or the singularity of the matrix R that contains the right eigenvectors (see discussions of (2.7)-(2.10)), the component-wise WENO reconstruction is adopted. For a detailed account of the WENO scheme, see [9,16,17] or [23,28], which are more relevant to the discussed model.

3.1 Component-wise finite volume (FV) WENO scheme

The fifth-order accurate WENO FV scheme applies the cell averages $\{(u_j, \theta_j)\}_{j=i-2}^{i+2}$ to reconstruct $(u_{i+1/2}^-, \theta_{i+1/2}^-)$, which are cell boundary values of $x_{i+1/2}$ on the left-hand side. With $\{(u_j, \theta_j)\}_{j=i-1}^{i+3}$, $(u_{i+1/2}^+, \theta_{i+1/2}^+)$ are similarly constructed, and are cell boundary values of $x_{i+1/2}$ on the right-hand side. Thus, we use the Lax-Friedrichs numerical fluxes as follows:

$$\hat{f}_{i+1/2} = \frac{1}{2}(f(u_{i+1/2}^-) + f(u_{i+1/2}^+) - \alpha(u_{i+1/2}^+ - u_{i+1/2}^-))$$

$$\hat{o}_{i+1/2} = -\frac{1}{2}\alpha(\theta^+_{i+1/2} - \theta^-_{i+1/2}). \tag{3.3}$$

Eqs. (3.3) and (3.2) constitute a complete semi-discretized scheme.

3.2 Component-wise finite difference (FD) WENO scheme

In this scheme, we first use the Lax-Friedrichs flux splitting as follows:

$$f^+ = \frac{1}{2}(f(u,\theta) + \alpha u), \quad f^- = \frac{1}{2}(f(u,\theta) - \alpha u);$$

$$o^+ = \frac{1}{2}\alpha\theta, \quad o^- = -\frac{1}{2}\alpha\theta, \tag{3.4}$$

where $(u,\theta) = (u_j,\theta_j)$, $j = i-2,\ldots,j+3$. With $(f^+_j, o^+_j) = (f^+(u_j,\theta_j), o^+(\theta_j)) \equiv v_j$ for $j = i-2,\ldots,i+2$, we proceed with the WENO reconstruction in the cell I_i to obtain $v^-_{i+1/2}$, and then set $(\hat{f}^+_{i+1/2}, \hat{o}^+_{j+1/2}) = v^-_{i+1/2}$. Similarly, with $(f^-_j, o^-_j) = (f^-(u_j,\theta_j), o^-(\theta_j)) \equiv v_j$ for $j = i-1,\ldots,i+3$, we proceed with the WENO reconstruction in the cell I_{i+1} to obtain $v^+_{i+1/2}$, and then set $(\hat{f}^-_{i+1/2}, \hat{o}^-_{j+1/2}) = v^+_{i+1/2}$. The numerical fluxes are thus given by

$$\hat{f}_{i+1/2} = \hat{f}^+_{i+1/2} + \hat{f}^-_{i+1/2}, \quad \hat{o}_{i+1/2} = \hat{o}^+_{i+1/2} + \hat{o}^-_{i+1/2}. \tag{3.5}$$

Eqs. (3.5) and (3.2) give the scheme.

In (3.3) and (3.4), $\alpha \equiv \max\limits_{(u,\theta)} \max\limits_{1\le l\le m} |\lambda_l(u,\theta)|$. As all of the λ_l are implicit, a slightly larger estimation of α is made according to (2.7):

$$\alpha = \max_{(u,\theta)} \max(|v_1 + \sum_{l=1}^{m} \rho_l \frac{\partial v_l}{\partial \rho}|, |v_m|).$$

The maximum is taken over the relevant region of $(u,\theta) = (u_j,\theta_j)$ for all j.

Finally, we apply the third-order accurate TVD Runge-Kutta time discretization [7], for which the semi-discrete scheme (3.2) is written as the ODEs

$$u_t = L(u,\theta).$$

For the numerical stability of the described WENO scheme, considerable numerical experience suggests the following CFL condition [6]:

$$\alpha^{(n)} \frac{\Delta t^{(n)}}{\Delta x} \le CFL,$$

where CFL can be taken as 0.6. Note that $\Delta t^{(n)}$ and $\alpha^{(n)}$ are corresponding values at time level n.

4 Numerical examples

In Section 4.1, numerical tests are conducted to determine the waves that are described in Section 2.2. The traffic that approaches the stop line of a traffic signal is simulated in Section 4.2. These examples are computed using the component-wise FD WENO scheme. We note that the component-wise FV WENO scheme generates similar results.

For a clear observation of these waves, the velocities of (1.1) are set to be linear [8,22],

$$v(\rho) = v_f(1 - \frac{\rho}{\rho_{jam}}).$$

In all of the illustrations, the densities ρ_l and ρ are scaled by ρ_{jam} so that $0 \leq \rho_l, \rho \leq 1$, and the spatial and temporal lengths L and T of the computational domain $(0, L) \times (0, T)$ are scaled to unity. These dimensionless variables are also used wherever they are not followed by a unit.

4.1 Resolution of the waves compared to the analytical results

The initial data in this section are given by the Riemann problem (2.11), with the translation of $x = 0$ to $x = x_0$ somewhere in $(0, L)$. Furthermore, we set $m = 3$, which is small enough for a clear observation of the wave breaking. For simplicity, $b_l(x)$ are set to be constant for all l, namely,

$$b_1(x) = 0.5, \quad b_2(x) = 0.75, \quad b_3(x) = 1. \tag{4.1}$$

The other parameters are

$$L = 8000m, \quad T = 400s, \quad \Delta x = 10m, \quad \text{and} \quad \Delta t^{(n)} = 0.6\Delta x/\alpha^{(n)},$$

where T is the simulation time.

Figs.3-10 show the numerical results, which are designed to reproduce all of the analytical wave patterns in Section 2.2, and to confirm Propositions 2.1 and 2.2. In each figure, we observe the waves as follows.

First, we count the wave number. Four $(m + 1)$ waves are observed in Figs.3-6 that correspond to the wave patterns that are described in **(1)**(a), (b), and (c) and illustrated in Figs.1 (a) and (b). In these cases, the system is strictly hyperbolic. In Figs.7-10, there are five $(m + 2)$ waves, which correspond to the wave patterns that are described in **(2)**(a), (b), and (c) and illustrated in Figs.2(a) and (b). In these cases, the system must be non-strictly hyperbolic.

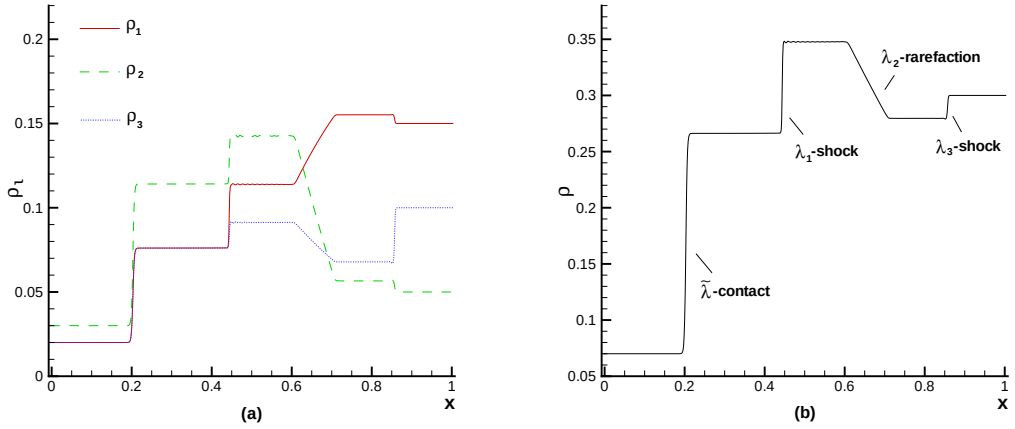

Fig.3 Wave pattern (1)(a) with $x_0 = 0.2$, $a^L = 3$, $a^R = 1$, $u^1/a^L = (0.02, 0.03, 0.02)^T$, and $u^{m=1}/a^R = (0.15, 0.05, 0.1)^T$ as compared with Fig.1(a). (a) density ρ_l; (b) total density ρ.

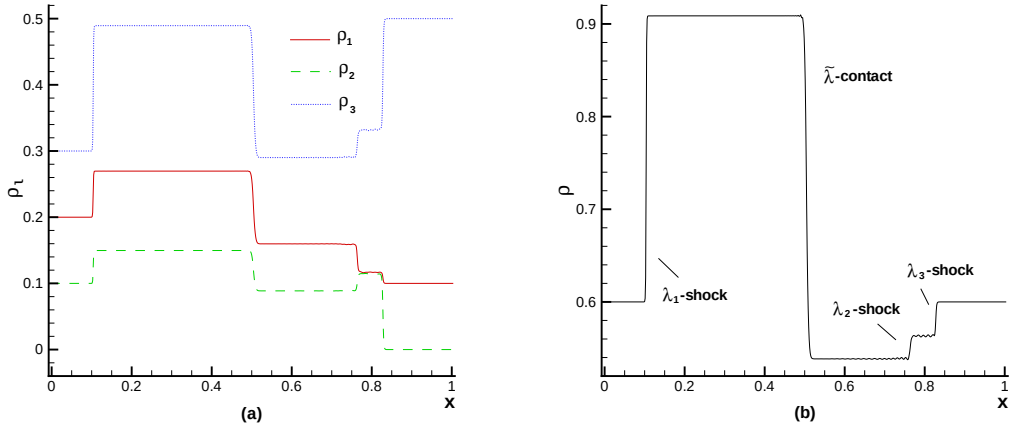

Fig.4 Wave pattern (1)(b) with $x_0 = 0.5$, $a^L = 3$, $a^R = 1$, $u^1/a^L = (0.2, 0.1, 0.3)^T$, and $u^{m+1}/a^R = (0.1, 0, 0.5)^T$ as compared with Fig.1(b). (a) density ρ_l; (b) total density ρ.

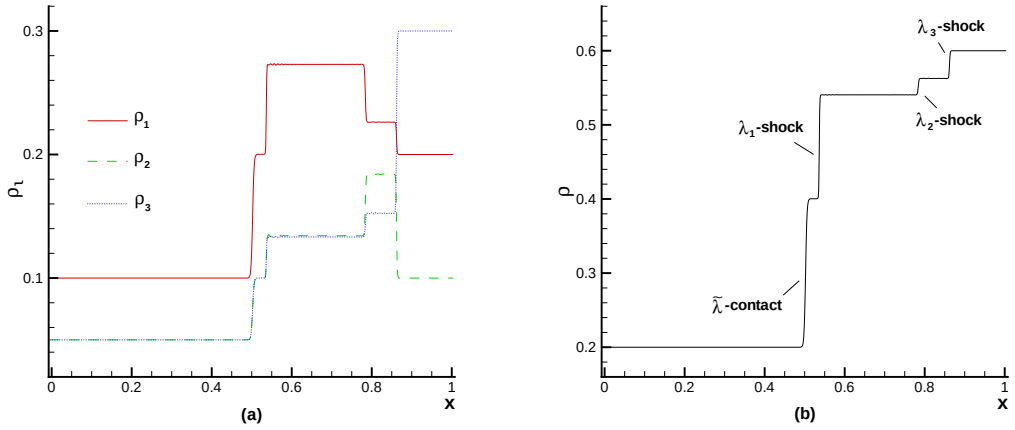

Fig.5 Wave pattern (1)(c) with $x_0 = 0.5$, $a^L = 3$, $a^R = 2$, $u^1/a^L = (0.1, 0.05, 0.05)^T$, and $u^{m+1}/a^R = (0.2, 0.1, 0.3)^T$ as compared with Fig.1(a). (a) density ρ_l; (b) total density ρ.

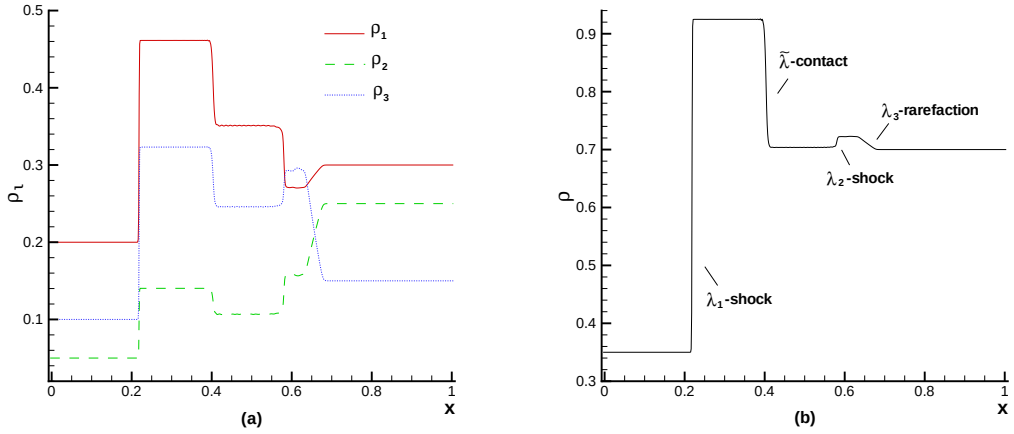

Fig.6 Wave pattern (1)(c) with $x_0 = 0.4$, $a^L = 3$, $a^R = 1$, $u^1/a^L = (0.2, 0.05, 0.1)^T$, and $u^{m+1}/a^R = (0.3, 0.25, 0.15)^T$ as compared with Fig.1(b). (a) density ρ_l; (b) total density ρ.

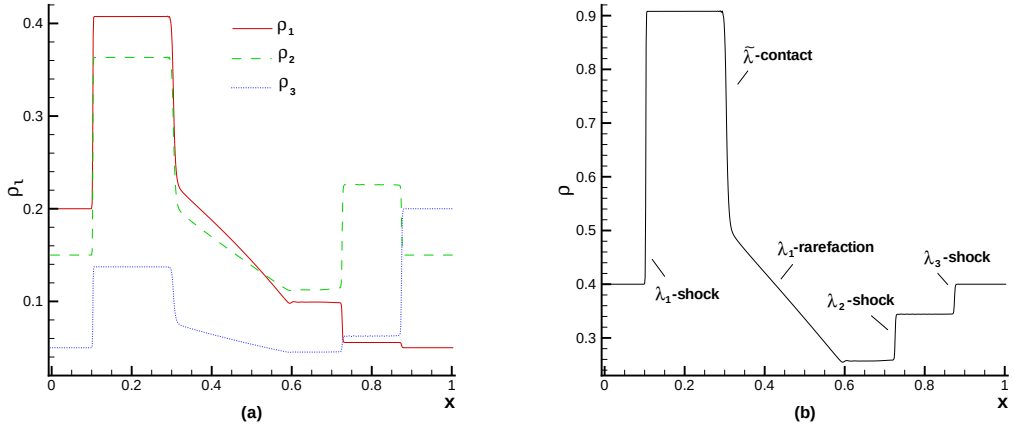

Fig.7 Wave pattern (2)(a) with $x_0 = 0.3$, $a^L = 3$, $a^R = 1$, $u^1/a^L = (0.2, 0.15, 0.05)^T$, and $u^{m+1}/a^R = (0.05, 0.15, 0.2)^T$ as compared with Fig.2(a). (a) density ρ_l; (b) total density ρ.

Secondly, we identify all of the λ_l-waves in each figure according to Propositions 2.1 and 2.2. We first observe the monotone change of the total density that is shown in the right part of the figure, such that each of these waves is identified to be either a shock or a rarefaction. Accordingly, as shown in the left part of the figure, the monotone changes for all density ρ_l across or in the same wave are observed and confirmed to be in accordance with Proposition 2.1 (for a shock) or Proposition 2.2 (for a rarefaction).

Thirdly, as shown in Figs.7(b)-10(b), we note that $\rho^R = \rho^* = 0.5$ (in Figs.7(b) and 9(b)) or $\rho^L = \rho^* = 0.5$ (in Figs.8(b) and 10(b)) for the λ_1-rarefaction. These are the analytical results of the wave breaking across the interface ($\tilde{\lambda}$-contact).

In summary, we claim that the numerical results that are given by the developed scheme are completely in accordance with the analytical properties that are predicted in Section 2.2.

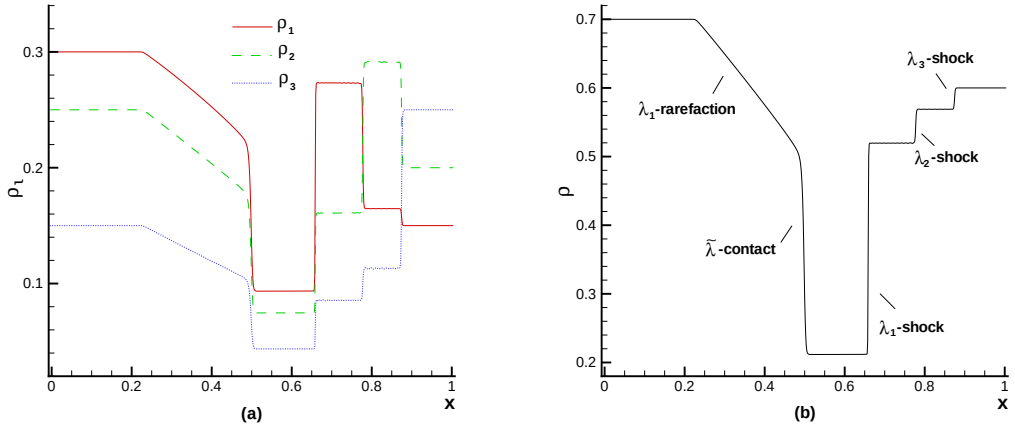

Fig.8 Wave pattern (2)(b) with $x_0 = 0.5$, $a^L = 2$, $a^R = 3$, $u^1/a^L = (0.3, 0.25, 0.15)^T$, and $u^{m+1}/a^R = (0.15, 0.2, 0.25)^T$ as compared with Fig.2(b). (a) density ρ_l; (b) total density ρ.

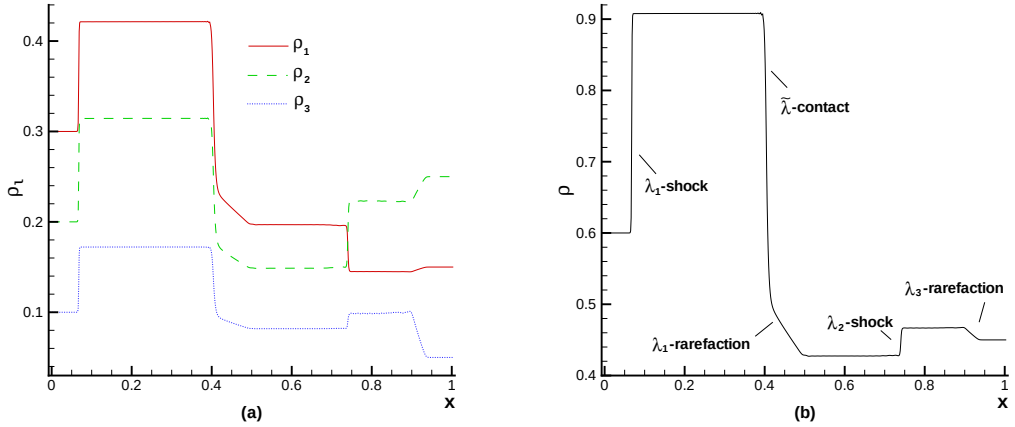

Fig.9 Wave pattern (2)(c) with $x_0 = 0.4$, $a^L = 3$, $a^R = 1$, $u^1/a^L = (0.3, 0.2, 0.1)^T$, and $u^{m+1}/a^R = (0.15, 0.25, 0.05)^T$ as compared with Fig.2(a). (a) density ρ_l; (b) total density ρ.

In this observation, we also note that $\lambda_1(u^2, \theta^R)$ and $\lambda_1(u^{m+1}, \theta^R)$ $(m = 3)$ share the same sign in all of the examples. This can be seen in Figs.3(b)-10(b)(by (2.9)) and should be true in general. Therefore, some of the predictions in Section 2.2 can also be made conveniently for the substitution of $\lambda_1(u^2, \theta^R)$ with $\lambda_1(u^{m+1}, \theta^R)$.

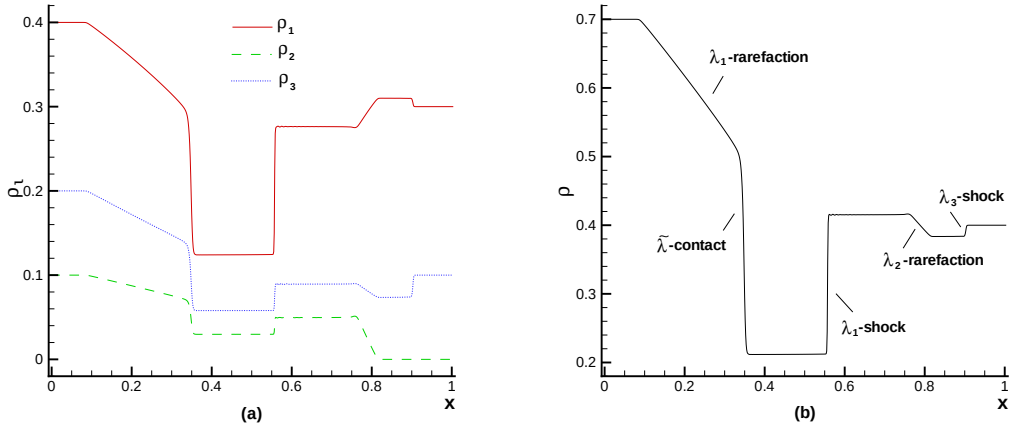

Fig.10 Wave pattern (2)(c) with $x_0 = 0.35$, $a^L = 2$, $a^R = 3$, $u^1/a^L = (0.4, 0.1, 0.2)^T$, and $u^{m+1}/a^R = (0.3, 0, 0.1)^T$ as compared with Fig.2(b). (a) density ρ_l; (b) total density ρ.

4.2 Traffic signal control

We extend the developed scheme to an application in which the functions of θ are also temporal. This is very common in traffic problems, and signal control is a typical example of the extension. At the stop line, the signal display turns from green to red (at $t = 0s$) and holds, for example, for 30 seconds, and then turns back to green for another 30 seconds. To reflect this regular change of traffic signal, which is near $x = 0.35$ on a road with a section length $L = 1200m$ and a constant $a(x)$, we suppose that all b_l $(m = 3)$ are given by (3.6) for the green signal, but are zero near $x = 0.35$ and for the red light, as is described by the following:

$$(b_1, b_2, b_3) = \begin{cases} (0,0,0), & if \quad 0.34 < x < 0.36, \ and \ 0 < t - 60[t/60] \le 30s, \\ (0.5, 0.75, 1). & otherwise. \end{cases} \tag{4.2}$$

For the initial condition:

$$u(x,0)/a = (0.05, 0.25, 0.1)^T. \tag{4.3}$$

The numerical result is shown in Fig.11.

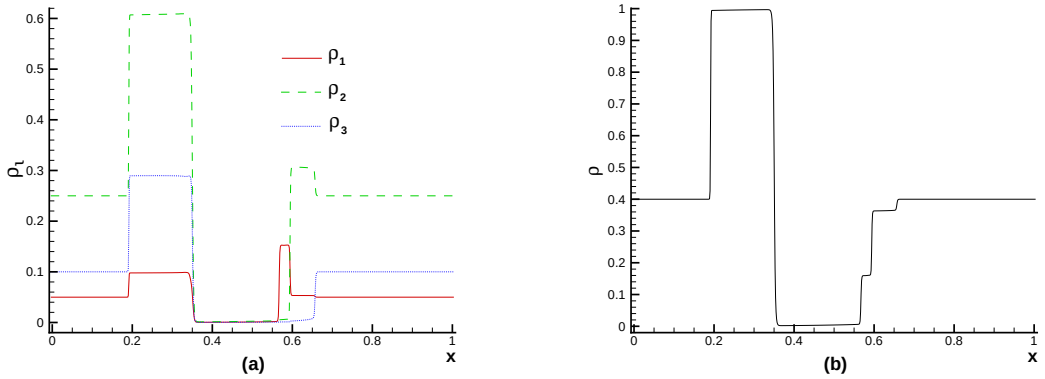

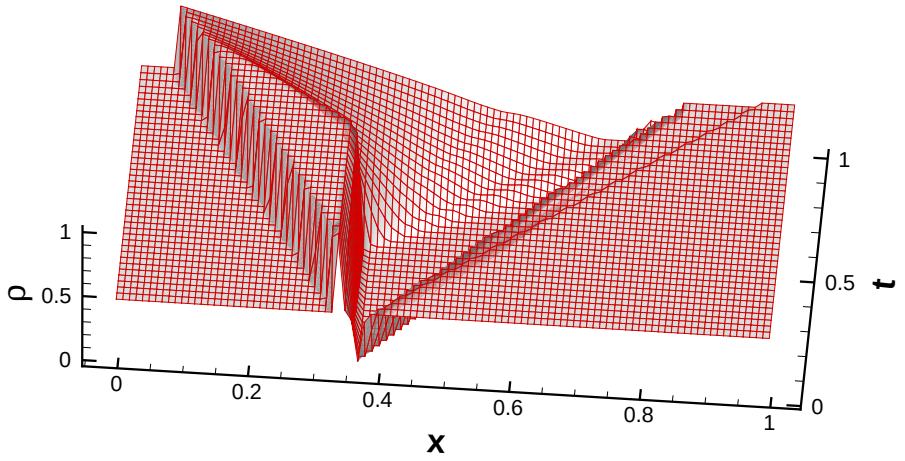

(c)

Fig.11 Traffic states during a signal cycle that is controlled by (4.2). The initial data are given by (4.3) and the other parameters are $\Delta x = 1.5m$ and $\Delta t^{(n)} = 0.3\Delta x/\alpha^{(n)}$. (a) Densities of all classes at $t = 30s$; (b) total density at $t = 30s$; (c) change of total density for the simulation time $T = 60s$.

We also set

$$(b_1, b_2, b_3, b_4, b_5) = \begin{cases} (0,0,0,0,0), & if \;\; 0.34 < x < 0.36, \;\; and \; 0 < t - 60[t/60] \leq 30s, \\ (0.6, 0.7, 0.8, 0.9, 1). & otherwise, \end{cases} \tag{4.4}$$

and

$$u(x,0)/a = (0.15, 0.05, 0.1, 0.05, 0.05)^T. \tag{4.5}$$

The numerical result for this case is shown in Fig.12.

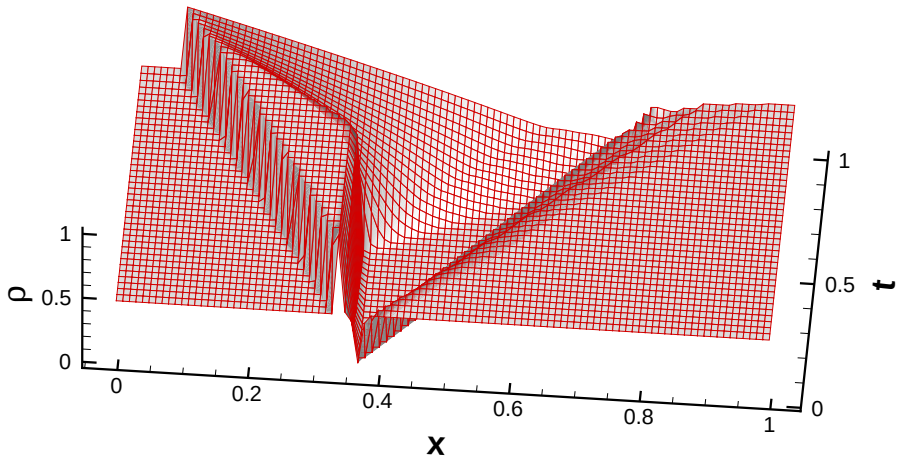

Fig.12 Change of total density for the simulation time $T = 60s$ during a signal cycle that is controlled by (4.4). The initial data are given by (4.5) and the other parameters are $\Delta x = 1.5m$ and $\Delta t^{(n)} = 0.3\Delta x/\alpha^{(n)}$.

5 Conclusion

With the modified system, this numerical test of the multi-class traffic flow model on an inhomogeneous highway shows the robustness of the WENO reconstruction when combined with the Lax-Friedrichs flux splitting or Lax-Friedrichs numerical flux. Based on this standard hyperbolic conservation system (despite it being non-strictly hyperbolic), the Lax-Friedrichs flux gives correct numerical viscosity for the convergence of the numerical solutions to physically relevant solutions, whereas the WENO reconstruction reduces the surplus numerical viscosity to achieve a high level of resolution of the claimed waves. This again indicates the robustness of the WENO reconstruction, especially when it is combined with the Lax-Friedrichs flux to solve many complexities in application problems.

The application of the WENO scheme in this paper can be extended to solve other hyperbolic conservation laws with spatially varying fluxes, such as elastic waves in heterogeneous media. It would also be interesting to investigate the use of other well-known numerical schemes, such as the RKDG scheme [3-5].

References

[1] P. Baiti and H. K. Jenssen, Well-posedness for a class of 2×2 conservation laws with L_∞ data, Journal of Differential Equations 140 (1997), 161-185.

[2] D. B. Bale, R. J. LeVeque, S. Mitran, and A. Rossmanith, A wave propagation method for conservation laws and balance laws with spatially varying flux functions, SIAM Journal of Scientific Computing 24 (2002), 955-978.

[3] B. Cockburn and C. W. Shu, TVB Runge-Kutta local projection discontinuous Galerkin finite element method for conservation laws II: General framework, Mathematics of Computation 52 (1989), 411-435.

[4] B. Cockburn and C. W. Shu, The Runge-Kutta local projection P-discontinuous Galerkin methods for scalar conservation laws. Modelisation Mathematique et Analyse Numerique 25 (1991), 337-361.

[5] B. Cockburn, An introduction to the discontinuous Galerkin method for convection-dominated problems, in Advanced Numerical Approximation of Nonlinear Hyperbolic Equations, B. Cockburn, C. Johnson, C.-W. Shu and E. Tadmor (Editor: A. Quarteroni), Lecture Notes in Mathematics, volume 1697, Springer, 1998, pp. 151-268.

[6] S. Gottlieb, C.-W. Shu and E. Tadmor, Strong stability preserving high order time discretization method, SIAM Review 43 (2001), 89-112.

[7] C.-W. Shu and S. Osher, Efficient implementation of essentially non-oscillatory shock-capturing schemes, Journal of Computational Physics 77 (1988), 439-471.

[8] B. D. Greenshields, An analysis of traffic flow, Proceedings of the Highway Research Board 14 (1934), 448-477.

[9] G. Jiang and C.-W. Shu, Efficient implementation of weighted ENO schemes, Journal of Computational Physics 126 (1996), 202-228.

[10] R. A. Klausen, Stability of conservation laws with discontinuous coefficients, Journal of Differential Equations 157 (1999), 41-60.

[11] P. D. Lax, Hyperbolic systems of conservation laws II, Communications on Pure and Applied Mathematics 10 (1957), 537-566.

[12] P. D. Lax, Shock waves and entropy, Contributions to Nonlinear Functional Anal. Proc. Symposium at the University of Wisconsin, (1971) 603.

[13] P. D. Lax, Hyperbolic Systems of Conservation Laws and the Mathematical Theorey of Shock waves, SIAM, Philadelphia, 1973.

[14] R. J. LeVeque, Finite-volume methods for non-linear elasticity in heterogeneous media, International Journal for Numerical Methods in Fluids 40 (2002), 93-104.

[15] L. Lin, J. B. Temple and J. Wang, Suppression of oscillations in Godunov's method of a resonant non-strictly hyperbolic system, SIAM Journal of Numerical Analysis 32 (1995), 841-864.

[16] X.-D. Liu, S. Osher and T. Chan, Weighted essentially nonoscillatory schemes, Journal of Computational Physics 115 (1994), 200-212.

[17] C.-W. Shu, Essentially non-oscillatory and weighted essentially non-oscillatory schemes for hyperbolic conservation laws, in Advanced Numerical Approximation of Nonlinear Hyperbolic Equations, B. Cockburn, C. Johnson, C.-W. Shu and E. Tadmor (Editor: A. Quarteroni), Lecture Notes in Mathematics, volume 1697, Springer, 1998, pp. 325-432.

[18] I. Smoller, Shock Waves and Reaction-Diffusion Equations, Springer-Verlag, New York, 1994.

[19] E. F. Toro, Riemann Solvers and Numerical Methods for Fluid Dynamics, Springer-Verlay, 1999.

[20] G. B. Whitham, Linear and Nonlinear Waves. NY: John Wiley and Sons, 1974.

[21] G. C. K. Wong and S. C. Wong, A multi-class traffic flow model - an extension of LWR model with heterogeneous drivers, Transportation Research 36A (2002), 827-841.

[22] S. C. Wong and G. C. K. Wong, An analytical shock-fitting algorithm for LWR kinematic wave model embedded with linear speed-density relationship, Transportation Research 36B (2002), 683-706.

[23] M. P. Zhang, C.-W. Shu, G. C. K. Wong and S. C. Wong, A weighted essentially non-oscillatory numerical scheme for a multi-class Lighthill-Whitham-Richards traffic flow model, Journal of Computational Physics 191 (2003), 639-659.

[24] P. Zhang and R. X. Liu, Hyperbolic conservation laws with space-dependent flux: I Characteristics theory and Riemann problem, Journal of Computational and Applied Mathematics 156 (2003), 1-21.

[25] P. Zhang and R. X. Liu, Hyperbolic conservation laws with space-dependent flux: II General study on numerical fluxes, Journal of Computational and Applied Mathematics 176 (2005), 105-129.

[26] P. Zhang and R. X. Liu, Generalization of Runge-Kutta discontinuous Galerkin method to LWR traffic flow model with inhomogeneous road conditions, Numerical Methods for Partial Differential Equations, 21 (2005), 80-88.

[27] P. Zhang, R. X. Liu, and S. C. Wong, High-resolution numerical approximation of traffic flow problems with variable lanes and free flow velocities, Physical Review E, forthcoming.

[28] P. Zhang, R. X. Liu, S. C. Wong, and S. Q. Dai, Hyperbolicity and kinematic waves of a class of multi-population partial differential equations, European Journal of Applied Mathmetical, forthcoming.